



The effect of artificial ageing heat treatments on the corrosion-induced hydrogen embrittlement of 2024 (Al–Cu) aluminium alloy



Nikolaos D. Alexopoulos^{a,*}, Zaneta Velonaki^a, Constantinos I. Stergiou^b, Stavros K. Kourkoulis^c

^a University of the Aegean, Department of Financial Engineering, 821 00 Chios, Greece

^b Technological Educational Institute of Piraeus, Department of Mechanical Engineering, 250 Thivon Ave, 12244 Athens, Greece

^c National Technical University of Athens, Department of Mechanics, Laboratory of Testing and Materials, 9 Heroon Polytechniou Str., 15780 Athens, Greece

ARTICLE INFO

Article history:

Received 19 August 2015

Received in revised form 21 October 2015

Accepted 23 October 2015

Available online 28 October 2015

Keywords:

A. Aluminium

A. Alloys

B. SEM

C. Exfoliation corrosion

C. Hardening

C. Pitting corrosion

C. Hydrogen embrittlement

ABSTRACT

This work is focused on the role of microstructure (*S*-type particles) that are precipitated in the aluminium matrix due to artificial ageing on the tensile ductility decrease of 2024 aluminium alloy when exposed to exfoliation corrosion solution. A common, extremely short corrosion exposure time was selected to corrode the already heat-treated specimens in different conditions, including under-, peak- and over-ageing so as to avoid pitting formation and to concentrate only to hydrogen embrittlement degradation. Corrosion-induced yield stress decrease was less sensitive to the change of microstructure. Corrosion-induced tensile ductility decrease was correlated with the precipitation of *S*-phase particles, showing that the specimens at the peak-ageing (*S''* and *S'* precipitates) and over-ageing (*S* precipitates) exhibited the lowest decrease (~11% and ~22%, respectively) due to corrosion exposure. The highest ductility decrease (~26%) was noticed for the T3 condition (as received) that limited GPB zones were formed on the grain boundaries. Tensile ductility decrease was also ageing temperature sensitive, as the lowest temperature gave the least ductility decrease, thus giving proof of the role of the precipitates on the corrosion mechanism. The results were explained based on the hydrogen trapping at the interphases of the *S*-type precipitates.

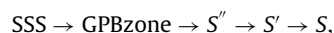
© 2015 Elsevier Ltd. All rights reserved.

1. Introduction

Many decades now, the aluminium alloy 2024 is widely used in the aeronautical industry due to its high specific mechanical properties and damage tolerance capabilities. New versions and derivatives of AA2024 with lower compositions of Fe and Si have been investigated during the last decade to improve fatigue, fracture toughness and resistance to corrosion. AA2024-T3 is a high strength alloy with a complex microstructure, comprising the aluminium matrix as well as a number of different intermetallic particles. Several articles tried to characterise the resulting microstructure of the alloy and the respective composition of the intermetallic particles [1,2]. Almost 61.3% of the intermetallic particles are *S*-phase (Al_2CuMg), 12.3% are $\text{Al}_6(\text{Cu,Fe,Mn})$, 5.2% are $\text{Al}_7\text{Cu}_2\text{Fe}$ and 4.3% are $(\text{Al,Cu})_6\text{Mn}$ particles in AA2024 [2].

Starke and Staley [3] suggested that, in addition to *S*-phase and θ -phase (Al_2Cu) particles, the intermetallic particles included AlCuFe and AlFeMnSi . In a recent work, Boag et al. [1] showed that the microstructure of AA2024-T3 is very complicated, exhibiting multiphase particles, periphery phases around composite particles and clustering. A shape-based classification of the particles was used to distinguish between $\text{Al}_{20}(\text{Cu,Mn,Fe})_5\text{Si}$ type particles and the rest intermetallic particles, however, this could not confidently be used to distinguish between cathodic and anodic particles. Hence, the authors suggested that a compositional classification would be appropriate, since it better reflects the likely electrochemical properties.

It is well known that AA2024 is strengthened by microstructure evolution (precipitates) during ageing. In the 1950s, Bagaryatsky [4] proposed the following precipitation sequence:



where SSS stands for supersaturated solid solution and GPB stands for Guinier–Preston–Bagaryatsky; GPB is considered to be a short

* Corresponding author.

E-mail address: nalexop@aegean.gr (N.D. Alexopoulos).

range ordering of Cu and Mg solute atoms while S' are very small precipitates fully coherent with the Al matrix. The S phase is an equilibrium phase and is incoherent with the Al matrix. These S -phase particles are round particles and 60% of the particles are larger than $0.5\ \mu\text{m}$ [2]. In contrast to the S -phase particles, the Al(Cu,Mn,Fe,Si) intermetallics present irregular shapes and size typically larger than $5\ \mu\text{m}$. The S' phase has generally been considered as semi-coherent with the matrix, having the same structure as the S -phase but with slightly different lattice parameters [4,5]. Ringer et al. [6,7] confirmed that GPB zones and other precipitate-structures prior to the S -phase formation are the dominant precipitates at the strengthening regime of the ageing curve, while the S -phase appears in the softening regime (over-ageing condition). In a most recent work, Wang and Starink [8] showed that actually two types of the S precipitate are formed, depending on the ageing temperature.

Recent studies for the corrosion of AA2024-T3 showed that the distribution of the second phase particles has a significant influence on the alloy corrosion behaviour. If the S -phase particles are preferentially cited at the grain boundaries, then copper depleted regions are developed adjacent to the boundaries. These are anodic to the copper rich grain boundaries, and hence, a micro-galvanic corrosion takes place that may cause corrosion of the particle, or corrosion of the surrounding matrix [9–14]. Corrosion of the Al_2CuMg phase with the surrounding matrix was also recently studied in the open literature [15,16]. Campestrini et al. [17] showed that a potential difference has been observed between the matrix and the intermetallic particles that result in the formation of a severe galvanic coupling. This weakens the natural oxide film of the aluminium alloy and explains the change of corrosion from general to localized, induced by the intermetallic particles. The effect of the precipitate size, the role of the nanostructure and the grain stored energy on the pitting potential in Al–Cu–Mg alloys are well documented [18–21].

In addition to the micro-galvanic corrosion associated with the grain boundary and its neighbouring regions, hydrogen embrittlement has been reported to be a contributing factor to the corrosion-induced degradation of mechanical properties in 2xxx aluminium alloys. Hydrogen production is a cathodic reaction during the corrosion process; recently in-situ X-ray tomography was used to capture H_2 production at the corrosion surface of AA2024 and the networks of intergranular corrosion extended into the material [22,23]. Larignon et al. [24] proposed that the grain and sub grain boundaries are preferential pathways for the diffusion of hydrogen. Hydrogen embrittlement has been reported to have an essential effect to the loss of tensile ductility of pre-corroded AA2024 [25–28]. Charitidou et al. [29] acknowledged that the diffused hydrogen is trapped in four sites in the microstructure of the alloy. The trapping states T1 and T2, were associated with the interstitial lattice sites [30] and with the semi-coherent interfaces of the strengthening phases or with the incoherent interphases of dispersoids and the matrix lattice, respectively. Scamans and Tuck [31] attributed the trap T3 to the formation of Mg hydride. The trapping site T4 began to release hydrogen at a temperature coinciding with the dissolution of the strengthening phase, thus implying that hydrogen is trapped inside/or at the interphase of this second phase [29]. Scholes et al. [32] also observed that the corrosion in alloy 2024-T3 was initiated at S -phase particles. Saitoh et al. [33] proved that the above microstructural features of the alloy can be used as hydrogen traps by employing tritium autoradiography.

In order to investigate the hydrogen embrittlement effect, a wide variety of methods to introduce hydrogen has been used over the years, such as cathodic charging [34], exposure to humid air as well as exposure to a corrosive environment. For the latter case, it is quite often the degradation mechanism to be a synergy of stress-concentration by the corrosion-induced surface pits and subsequent micro-cracking as well as of hydrogen embrittlement.

For example, Alexopoulos and Papanikos [27] performed fracture toughness mechanical tests on the same alloy and for various exposure times to corrosive environment. They have shown that the total reduction of almost 30% of the fracture toughness after 96 h exposure to exfoliation corrosion solution was attributed primary to the reduction of the alloy effective thickness (22%) and secondary to the hydrogen embrittlement (8%) mechanism. Hence, in order to assess the true hydrogen embrittlement effect, short exposure times should be selected to corrode the specimens so as to prevent the formation of corrosion-induced surface pits that act as stress raisers and degrade the ductility of the alloy.

It is evident though, that the tensile mechanical properties of the material due to the precipitation hardening are a function of artificial, and hence, of natural ageing. An assessment of different artificial ageing conditions to the corrosion-induced degradation on mechanical properties should be attempted. To the authors knowledge, quite a few researchers [34–38] tried to assess the effect of different artificial ageing conditions to the corrosion potential of AA2024. Zhang and Frankel [39] also studied the pitting and intergranular corrosion behaviour of various tempers of AA2024. Artificial ageing was found to have a strong effect on polarization curves and localized corrosion morphology of AA2024; it resulted in more precipitation of intermetallic particles from the matrix and formation of Cu-depleted matrix phase, which greatly changed the localised corrosion of AA2024. In the ASM Handbook [40], it is generally reported that the 2xxx wrought aluminium alloys in the T3 condition have low corrosion resistance when compared to the “precipitated” T6 and T8 conditions of the alloy. In a most recent article, Alexopoulos [28] demonstrated that for different artificial ageing conditions and subsequent exfoliation corrosion exposure for 24 h exposure time, the aged AA2024 specimens presented higher corrosion resistance than the T3 condition.

In the present work, the effect of artificial ageing of AA2024-T3 on the tensile mechanical properties degradation due to corrosion exposure will be investigated. Tensile specimens will be artificially aged to tempers that correspond to Under-Ageing (UA), Peak-Ageing (PA) and Over-Ageing (OA) conditions and then will be subsequently exposed to exfoliation corrosion environment. The corrosion exposure will be experimentally derived and should be the least possible so as to avoid the formation of large surface pits, trying to simulate the hydrogen embrittlement phenomenon. The purpose of this work is to identify how the resulting microstructure from artificial ageing affects the pitting corrosion potential, hydrogen embrittlement and corrosion-induced degradation of the tensile mechanical properties.

2. Material and specimens

The materials used for the present investigation were AA2024-T3 wrought aluminium alloy that was received in sheet form with nominal thicknesses of 3.2 mm and without any surface corrosion protection (Alclad). The sheets had geometrical dimensions of $35 \times 50\ \text{cm}$, while their thickness is typical for aerostructures. The weight percentage chemical composition of the alloy is 0.50% Si, 0.50% Fe, 4.35% Cu, 0.64% Mn, 1.50% Mg, 0.10% Cr, 0.25% Zn, 0.15% Ti and Al rem. Tensile specimens were machined from the longitudinal (L) direction of the material according to ASTM E8 specification with $12.5\ \text{mm} \times 3.2\ \text{mm}$ being the reduced cross-section and 50 mm being the gauge length of the specimens.

3. Experimental procedure

The experimental procedure flow diagram can be seen in Fig. 1; tensile specimens were machined, surface-cleaned with alcohol according to ASTM G1 and then were all artificially aged,

Download English Version:

<https://daneshyari.com/en/article/1468454>

Download Persian Version:

<https://daneshyari.com/article/1468454>

[Daneshyari.com](https://daneshyari.com)